Pergamon

Int. J. Heat Mass Transfer. Vol. 41, No. 15, pp. 2399–2407, 1998

Printed in Great Britain
0017–9310/98 $19.00+0.00

PII: S0017–9310(97)00299–8

Modeling of non-uniform heat dissipation and prediction of hot spots in power transistors

L. ZHU and K. VAFAI†
Department of Mechanical Engineering

and

L. XU
Department of Electrical Engineering, The Ohio State University, Columbus, OH 43210, U.S.A.

(*Received* 9 *May* 1997 *and in final form* 24 *September* 1997)

Abstract—In this work a heat generation model induced by current crowding is proposed. This model, in turn, is applied to the thermal calculation of typical multi-finger emitter structures of BJTs. The internal temperature distribution obtained from this model provides clear indication of the existence of hot spots in base-emitter contact region. The characteristics of the location and the magnitude of hot spots are also presented in this paper. Various pertinent effects due to the non-uniform heat dissipation are discussed. The result of this study serves to locate potential hot spots, which must be considered to prevent thermal breakdown of power BJTs as well as other types of power devices. © 1998 Elsevier Science Ltd. All rights reserved

1. INTRODUCTION

Contemporary power semiconductor devices are known to generate high heat flux up to 100 W cm^{-2}. This heat dissipation increases substantially with the current/voltage handling capability, operation frequency and the scaling-down of the device size. As a consequence of the intense heat dissipation, modern power devices operate at a high internal temperature. In most cases, heat distributes unevenly, causing localized high temperature regions, known as hot spot, within the power semiconductor devices. The maximum temperature in hot spots is likely to exceed an intrinsic temperature, at which the intrinsic carrier density equals to the dopant carrier density, thus causing transistor devices to fail its function and leading to possible thermal runaway. In order to understand this problem, the prediction of hot spots becomes crucial in the thermal design of integrated circuits (IC).

Due to the emitter current crowding in discrete and monolithic power transistor devices such as bipolar junction transistors (BJTs), Joule heating occurs mainly at the base-emitter contact rather than distributing uniformly within transistor devices. This non-uniform heat dissipation causes hot spots and leads to thermal runaway phenomena. Previous works in thermal modeling of these types of power transistors have not addressed this problem. In power devices such as BJTs, current crowding is an important cause of hot spots. Current crowding is caused by the lateral base-emitter (BE) current flowing from the base to the emitter. Due to the two-dimensional structure of power BJT devices and the sizable base resistance, the base current creates a lateral voltage drop between base-emitter contact region and the central emitter region. The voltage at the BE contact is higher than the voltage at the central emitter. As the current density increases exponentially with an increase of the applied voltage on a *pn* junction, the current density at the BE contact becomes drastically larger than the current density at the central emitter. This mechanism is known as the emitter current crowding, a commonly observed problem in power BJT devices. Corresponding to the non-uniform distribution of current density, the heat generation rate at the BE contact is also much larger than that at the central emitter, since heat dissipation rate is proportional to the current density. This non-uniform distribution of Joule heating induced by the emitter current crowding can produce potentially damaging hot spots.

Electrical effects of the current crowding have been investigated extensively in the solid state literature for semiconductors since the early years of transistor technology [1] and through the modern monolithic devices [2]. The classic model of Hauser [1] has been widely used as an analytical model which describes the distributed nature of emitter base junction voltage by introducing the concept of an equivalent base resistance. A recent extension of Hauser's model to the transient current crowding is given by Jin and Fossum in [3]. Thermal effects of current crowding,

† Author to whom correspondence should be addressed.

NOMENCLATURE

$\mathbf{e}$	electron charge, 1.6×10^{-19} [C]
$\mathbf{E}$	electric field vector [V cm^{-1}]
H	volumetric heat generation [W cm^{-3}]
I_{BE}^0	base current at base-emitter contact [A]
I_B	base current [A]
$\mathbf{J}$	current density vector [A cm^{-2}]
J_C	collector current density [A cm^{-2}]
J_S	reverse-bias current density [A cm^{-2}]
k	Boltzmann constant 1.38×10^{-23} [J K^{-1}]
N_a	acceptor doping density [cm^{-3}]
p	hole concentration [cm^{-3}]
T	internal temperature [K or °C]
V_{BE}	base-emitter potential [V]
V_{BE}^0	base-emitter potential at contact [V]
V_T	thermal voltage [V]
W_E	length of emitter-base finger [μm]
W_b	base thickness [μm]
x, y	coordinates [μm]
Z	current crowding parameter.

Greek symbols

θ	shape function
κ	thermal conductivity [W cm^{-1} K^{-1}]
μ_p	hole mobility [cm^2 V^{-1} s^{-1}]
ρ	base specific resistance [Ω cm^{-1}].

Subscripts

b, B	base
E	emitter
C	collector.

however, have been generally ignored in previous thermal modeling of power semiconductor devices, although the important issue of current crowding has been recognized and briefly discussed [4].

Two examples of the pertinent works about thermal modeling of transistor devices include works of Higgins [5] and Webb [6]. Higgins simulated the thermal behavior of Al/GaAs/As power Heterojunction Bipolar Transistors (HBTs) and established some quantitative tradeoff between power density, chip layout and junction temperature on multi-finger structures that is similar to the one studied in this paper. Likewise, Webb used the similar multi-finger structure for the thermal simulation of Gallium Arsenide HBTs and metal-semiconductor field effect transistors (MESFETs). In both of these works a uniformly distributed heat generation model was utilized and the current crowding effects was not considered. The exclusion of the current crowding effect in previous thermal studies stems from the inherent difficulty of modeling a complex coupled thermal-electrical phenomena.

As discussed earlier, the crowded current density at BE contact generates high heat dissipation rates, leading to hot spots. Hot spots substantially alter the semiconductor properties, increasing the intrinsic carrier density, which in turn increases the current density. This forms a positive feedback loop between current density and hot spots and makes the problem thermo-electrically coupled. One approach to this coupled problem is to simultaneously solve both the carrier transport equations as well as the energy equation [7] which usually involves a complex and a highly time-consuming simulation. Another approach which is adopted in this work is to obtain a semi-analytical formulation and to establish a heat generation model in which non-uniform distribution of Joule heating caused by current crowding is taken into consideration through an analytical model of lateral distributions of current density and junction voltage in the transistor.

2. MODELING OF THE HEAT GENERATION

In order to reduce current crowding, the emitters and the bases of practical power transistors are interleaved as narrow fingers, a part of which is shown in Fig. 1. The schematics of current crowding in one emitter strip is illustrated in Fig. 2. Figure 2(a) shows the lateral distribution of base current in a *npn* BJT. Usually the base region is moderately doped and is made relatively thin in order to obtain a large current gain. Consequently, there is a considerable base resistance which generates a lateral potential difference underneath the emitter region. In the *npn* BJT, this potential decreases from the BE contact towards the center of the emitter. The number of electrons injected

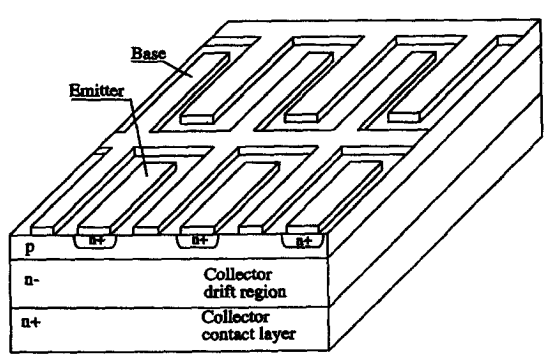

Fig. 1. Multi-finger structure of emitters and bases in power BJT transistors.

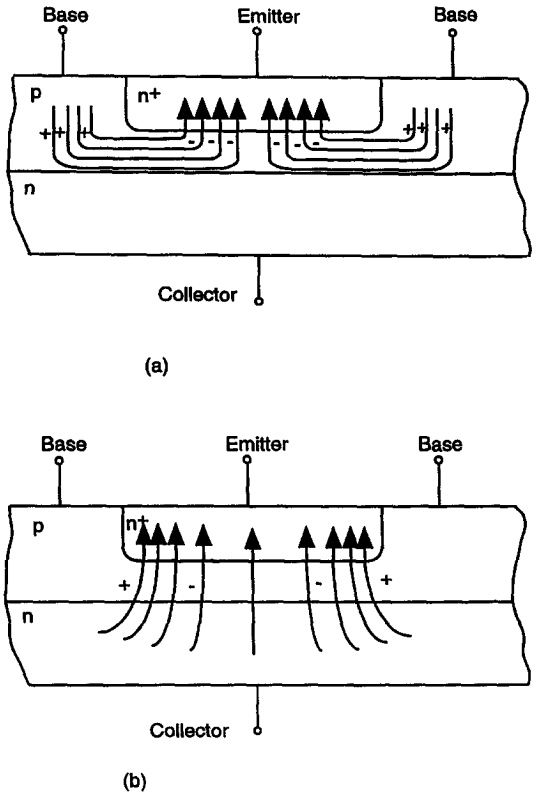

Fig. 2. Schematics of current crowding. (a) The lateral voltage drop induced by the base current. (b) The emitter current crowding.

from the emitter is exponentially dependent on the local BE voltage, so that more electrons are injected near the emitter boundary than at the center of the emitter, causing the crowding of the emitter current near the BE boundary. This results in current-crowding at the boundary as shown in Fig. 2(b). In addition, the substantial current density near the emitter boundary causes localized heating effects. To model this process, first, it should be noted that only one half of the BE finger structure needs to be analyzed (Fig. 3) since the base current distributes symmetrically with respect to the center of the emitter. The heat generation (power loss) in power transistors occurs when the device is at on-state, off-state and during switching transitions. Only the on-state Joule heating is accounted here as the off-state power loss due to the leakage current is usually negligible. The heat dissipation during switching transition, which is proportional to the switching frequency, is also not significant since BJTs normally are not high frequency devices [4]. The heat generation (Joule heating) in general is given by

$$H = \mathbf{J}\cdot\mathbf{E} = J_C\frac{V_{BE}(x)}{W_b} \tag{1}$$

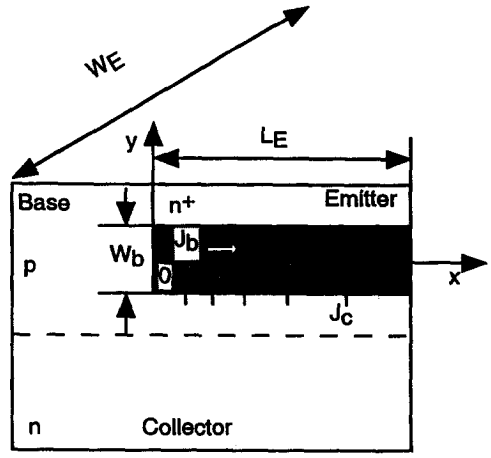

Fig. 3. One half of the base and emitter finger structure in BJTs.

where H is the Joule heat generation, $\mathbf{J}$ is the total current density vector and $\mathbf{E}$ is the electric field and J_C, $V_{BE}(x)$ and W_b define collector current density, BE junction voltage, and base thickness, respectively. The Joule heating dissipates mainly within the base region directly underneath the emitter (shaded area in Fig. 3). This is because the heavily doped emitter and the collector conduction layers have substantially smaller resistance compared to that of the base. Furthermore the resistance of the collector depletion region is also negligible when the BJT is at the on-state (forward active mode operation). The total current in the base includes the base current flowing laterally from the BE contact to the central emitter and the collector current flowing vertically from BE junction to the base-collector (BC) junction. The total current density is approximated as the collector current density J_C only, as indicated in the second part of equation (1). This is due to the fact that the magnitude of the lateral base current is much smaller than the collector current by a fraction of the common emitter gain. Note that the BE junction voltage, V_{BE}, is a function of position x due to the lateral distribution of base current.

The collector current density, when BC junction is forward biased, is given by the ambipolar diffusion theory as

$$J_C = J_S\left[\exp\left(\frac{V_{BE}(x)}{V_T}\right)-1\right] \approx J_S\exp\left(\frac{V_{BE}(x)}{V_T}\right) \tag{2}$$

where J_S is the reverse saturation current density of the base region. The thermal voltage, V_T, is defined as $V_T = (kt/\mathbf{e})$, with k being the Boltzmann constant, T, the temperature and $\mathbf{e}$, the electron charge. The BE junction voltage, V_{BE} can be written as

$$V_{BE} = V_{BE}^0 - \int_0^x J_B(\xi)\,\rho\,d\xi \tag{3}$$

where V_{BE}^0 is the BE voltage at BE contact, $x = 0$, I_B the base current and ρ is the effective specific resistance of the base which can be evaluated as

$$\rho = \frac{1}{2pe\mu_p W_E L_E} \tag{4}$$

in which p is the hole concentration in the p-doped base region which can be approximated as the base acceptor doping density N_a. The hole's mobility, μ_p, is assumed to be constant. The emitter length and the half emitter width, W_E and L_E, respectively, are shown in Fig. 3.

The majority part of I_B is the hole current that is back-injected from the base to the emitter, which is due to the recombination of excess minority carrier electrons with majority carrier holes at BE junction. I_B can thus be written as [1]

$$I_B(x) = I_B^0 - \int_0^x 2J_S W_E \left[\exp\left(\frac{V_{BE}(\xi)}{V_T}\right) - 1\right] d\xi$$

$$\approx I_B^0 - 2J_S W_E \int_0^x \exp\left(\frac{V_{BE}(\xi)}{V_T}\right) d\xi \tag{5}$$

where V_{BE} in equation (5) can be eliminated by differentiating equation (5) twice and utilizing equation (3). After some manipulation, we obtain the governing equation for I_B as

$$\frac{d^2 I_B}{dx^2} + \frac{\rho}{V_T} I_B \frac{dI_B}{dx} = 0. \tag{6}$$

For a *npn* BJT at the on-state, $I_B \geqslant 0$ and $(dI_B/dx) < 0$. In this case the general solution for equation (6) takes the following form

$$I_B(x) = C_1 \tan\left[\frac{C_1 \rho}{2V_T}(C_2 - x)\right] \tag{7}$$

where C_1 and C_2 are unknown constants to be determined from boundary conditions. One such boundary condition is the symmetry of I_B about the center of the emitter,

$$I_B(L_E) = 0. \tag{8}$$

Using equation (8), the two unknown constants C_1 and C_2 in equation (7) can be reduced to one parameter and equation (7) may be re-written as

$$I_B(x) = \frac{2V_T Z}{\rho L_E} \tan\left[Z\left(1 - \frac{x}{L_E}\right)\right] \tag{9}$$

where Z is the current crowding parameter. Another boundary condition is that at the BE contact, namely $x = 0$, we arrive at

$$I_B(0) = I_B^0 = \frac{2V_T Z}{\rho L_E} \tan(Z). \tag{10}$$

Substituting equation (9) in equation (5) we obtain an expression for V_{BE} in terms of Z

$$V_{BE}(x) = V_{BE}^0 - 2V_T \ln\left[\frac{\cos Z\left(1 - \frac{x}{L_E}\right)}{\cos Z}\right]. \tag{11}$$

In addition to equation (10), another expression for I_B^0 can be obtained by substituting equations (8) and (11) into equation (3). This results in

$$I_B^0 = W_E L_E J_S \exp\left(\frac{V_{BE}^0}{V_T}\right) \frac{\sin 2Z}{Z}. \tag{12}$$

Combining the two expressions, i.e. equations (10) and (12) for I_B^0. The constraint equation for the current crowding parameter Z is found to be

$$\frac{\cos^2 Z}{Z^2} = \frac{2V_T pe\mu_p W_b}{L_E^2 J_S} \exp\left(-\frac{V_{BE}^0}{V_T}\right). \tag{13}$$

It is not possible to measure V_{BE}^0 directly. However, it is possible to describe V_{BE}^0 in terms of the collector current for the entire BJT device which is controlled by the external circuit. The total collector current in the device can be written as

$$I_C = 2N_E W_E \int_0^{L_E} J_C(\xi)\, d\xi \tag{14}$$

where N_E is the effective number of emitter strips. The factor 2 in equation (14) accounts for the fact that only one half of the emitter strip is considered. Using equations (11) and (2) we can explicitly integrate equation (14). This results in

$$I_C = 2W_b N_E J_S \exp\left(\frac{V_{BE}^0}{V_T}\right) \int_0^{L_E} \frac{\cos^2 Z}{\cos^2\left[Z\left(1 - \frac{\xi}{L_E}\right)\right]} d\xi$$

$$= 2W_b N_E J_S \exp\left(\frac{V_{BE}^0}{V_T}\right) \frac{\sin Z}{Z}. \tag{15}$$

Combining equations (15) and (13) to eliminate the exponential term in equations (15) and (13), resulting in a constraint equation for Z,

$$\frac{Z \sin Z}{\cos^2 Z} = \frac{L_E I_C}{4kpe\mu_p W_b W_E N_E} \cdot \frac{1}{T} \tag{16}$$

and V_{BE}^0 can be given as

$$V_{BE}^0 = -V_T \ln\left(\frac{\cos^2 Z}{Z^2} \cdot \frac{L_E^2}{2kpe\mu_p W_b T}\right). \tag{17}$$

Finally substituting equations (15), (11), and (7) into equation (1), the heat generation model of BJTs which incorporates current crowding is attained as

$$H(x) = \frac{J_S}{W_b} V_{BE}(x) \frac{\cos^2 Z}{\cos^2\left[Z\left(1 - \frac{x}{L_E}\right)\right]} \exp\left(\frac{V_{BE}^0}{V_T}\right). \tag{18}$$

This heat generation model is applied to the energy equation to simulate the temperature distribution in the one-half base-emitter strip shown in Fig. 3. The relevant energy equation for the BJT is

$$\kappa(T)\left(\frac{\partial^2 T}{\partial x^2}+\frac{\partial^2 T}{\partial y^2}\right)+H(T)=0 \tag{19}$$

where κ is the silicon thermal conductivity that varies considerably with temperature. A temperature dependent model for κ which is given by

$$\kappa(T)=\frac{1}{3\times 10^{-4}+1.56\times 10^{-5}T+1.65\times 10^{-8}T^2} \tag{20}$$

is adopted in this work to account for this variation.

3. NUMERICAL METHODOLOGY

The governing equations are discretized using a finite element procedure. Temperature within each element is interpolated by linear functions, expressed in terms of temperatures to be determined at the four nodes as

$$T=\theta^T\mathbf{T}^{(e)} \tag{21}$$

where θ is the shape function and $\mathbf{T}^{(e)}$ is the nodal temperature array. The Galerkin form of the Method of Weighted Residuals is used to reduce the error introduced during the discretization process to zero, by making the residuals orthogonal to the interpolation function. The resulting discretization equation is

$$\mathbf{K}(T)\mathbf{T}=\mathbf{Q}+\mathbf{H}(T) \tag{22}$$

where $\mathbf{K}$, $\mathbf{Q}$ and $\mathbf{H}$ are stiffness matrix, load array from heat flux boundary condition and load array from heat source, respectively. They are defined as

$$\begin{aligned}\mathbf{K}(T)&=\sum_{i=1}^{n_e}\int_{V_e}\kappa(T)\frac{\partial\theta}{\partial x_j}\frac{\partial\theta^T}{\partial x_j}\mathrm{d}V\\ Q&=\int_{S_q}q\theta\,\mathrm{d}s\\ \mathbf{H}(T)&=\sum_{i=1}^{n_e}\int_{V_e}-H(T)\theta\,\mathrm{d}V.\end{aligned} \tag{23}$$

It should be noted that $\mathbf{K}$ and $\mathbf{H}$ are temperature dependent. A successive substitution procedure is used to solve equation (22). At every iteration step n, κ is updated with $T^{(n)}$ through the use of equation (20). The value of Z is obtained by solving equation (16). The values for V_{BE}^0 and V_{BE} are obtained through the use of equations (11) and (17), respectively, while H is calculated from equation (18). The updated value, $T^{(n+1)}$, is then obtained from

$$\mathbf{K}(T^{(n)})\mathbf{T}^{(n+1)}=\mathbf{Q}+\mathbf{H}(T^{(n)}). \tag{24}$$

This iterative procedure continues until the iteration criteria is satisfied. An advantage of this method is its fairly large convergent radius, which is essential for this nonlinear problem. The application of the Galerkin-based FEM is described by Taylor and Hood [8], and its application in the finite element program used in the present work is well documented [9].

4. RESULTS AND DISCUSSIONS

The simulations in this work are based on an actual BJT transistor used in power electronics applications. Three monolithical BJT structures are connected serially to form a Darlington structure for a multiplied current gain, as shown in Fig. 4. Most of the heat dissipation occurs in the third BJT (the main amplifier) as the current in that BJT is the largest. The effective number of emitter strips of the third BJT is set at 25. The base is usually moderately doped and N_a is approximated as 10^{16} cm^{-3} as a typical doping level. The length of the emitter is 500 μm and the thickness of the base is 8 μm. The rated collector current of a typical BJT device is set at 100 A. Various I_C values have been used in this simulation to study corresponding effect on the heat generation model as well as on the temperature distribution. The hole mobility μ_p is taken to be 480 cm^2 V^{-1}-s which is a typical value for BJTs. The leakage current J_S in the model includes the reverse saturation current and the reverse recombination current. It is taken as 1.8×10^{-8} A cm^{-2} again a typical value. The distribution of V_{BE} is shown in Fig. 5. From the center of the emitter to the BE contact, V_{BE} increases gradually from 0.58 V to 0.64 V across most of the base region and then rises rapidly from 0.64 V to 0.89 V within a distance of about 10 μm near BE boundary. Because of the exponential dependence of the injected electrons on V_{BE}, the rapid increase of V_{BE} in the thin layer near BE contact corresponds to a drastic increase in the current density and hence results in significant heat dissipation in this region.

A parametric study of the heat generation model given in equation (18) has been made. The parameters whose influence have been studied include the total collector current of the device, I_C, the emitter stripe width $2L_E$, and the internal temperature. Figure 5 also shows the lateral distribution of the heat generation for different collector currents. The internal temperature is assumed to be 80°C, a typical operation temperature of actual power transistors. Two observations of the heat generation rate distribution shown in Fig. 6 are worthy to be presented. First, we find that the heat dissipated in the BJTs is to a large degree concentrated on the BE boundary, contrasting the uniform distribution models that previous thermal investigations have assumed. In fact, the maximum heat dissipation rate near the BE boundary is about $3\sim 5\times 10^4$ times larger than the minimum heat dissipation rate occurring at the central emitter region.

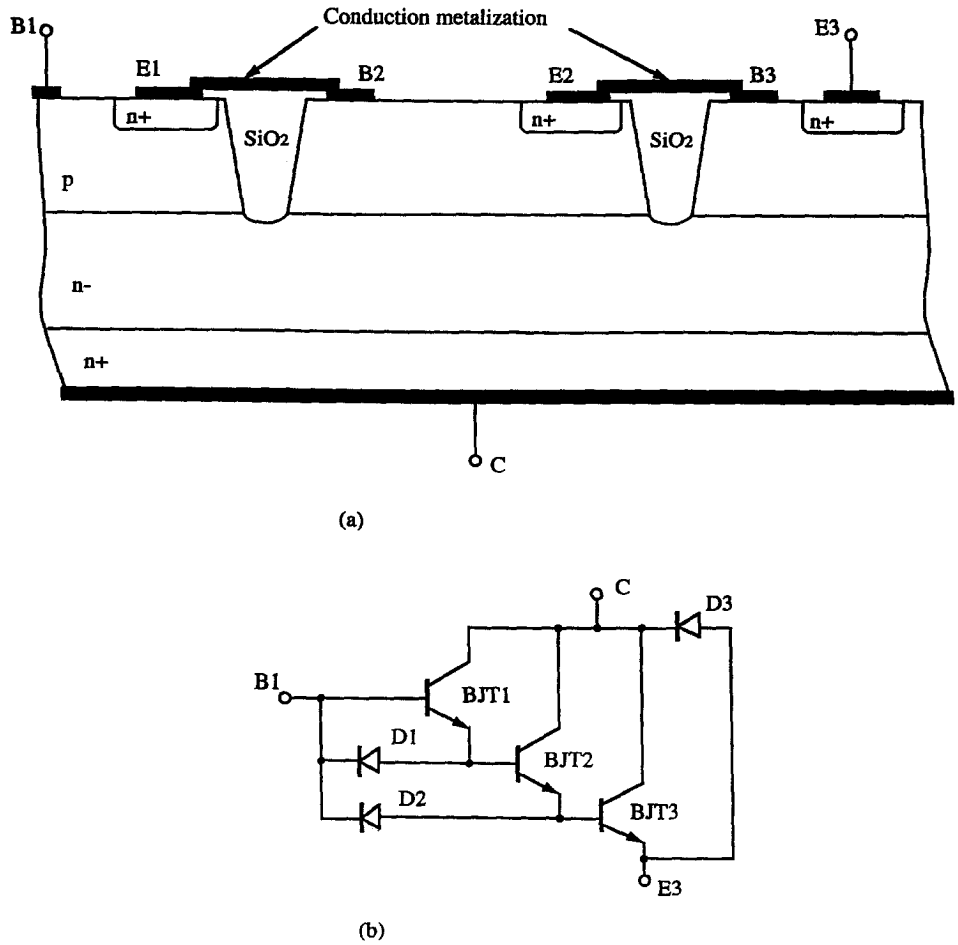

Fig. 4. Three Darlington-connected BJTs in a typical device. (a) Structure of three Darlington-connected BJTs. (b) Simplified circuit of three Darlington-connected BJTs.

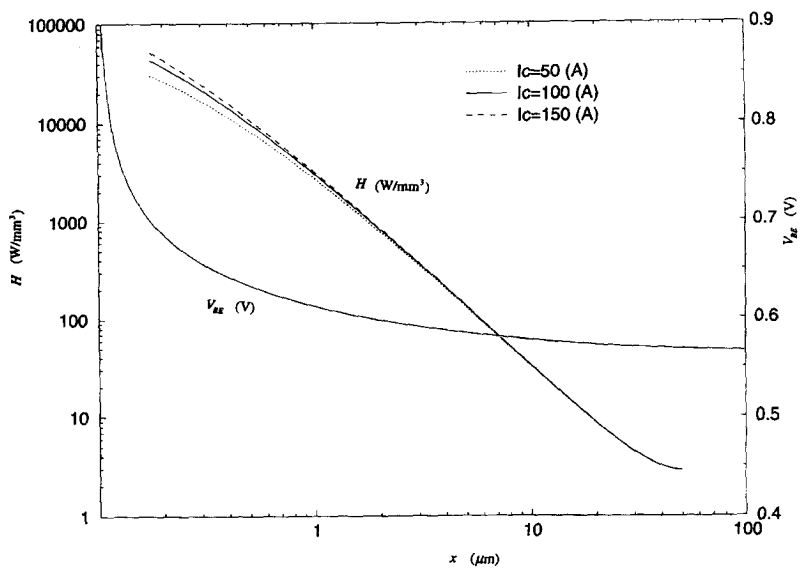

Fig. 5. Distribution of the heat dissipation rate H and the base-emitter voltage $V_{BE}(x)$.

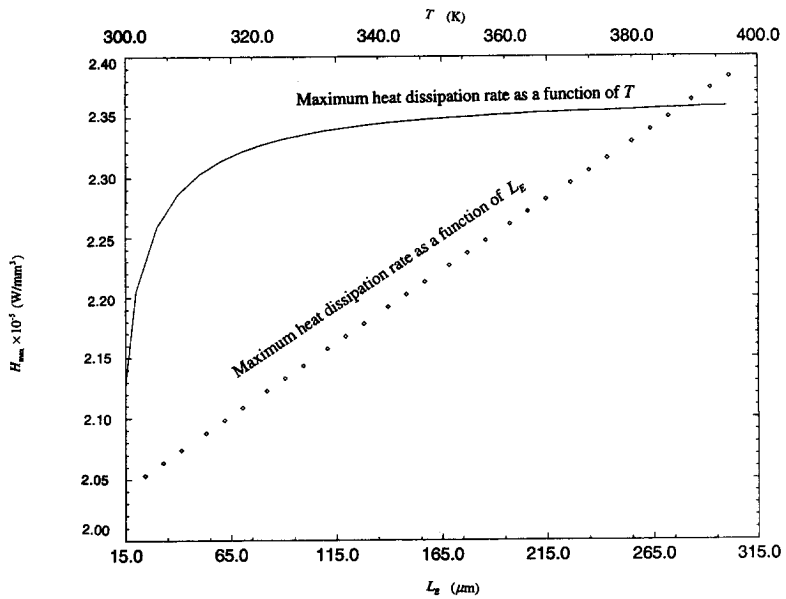

Fig. 6. Maximum heat dissipation rates as functions of temperature T and emitter half width, L_E.

Second, we observe from Fig. 5 that the maximum heat dissipation rate increases linearly with I_C at BE boundary but remains almost constant at the emitter center.

Another important parameter is $2L_E$, the half width of emitter strip. Figure 6 shows the change of maximum heat dissipation rate as a function of $2L_E$. The collector current and the temperature used in the calculation of Fig. 6 are 100 A and 80°C, respectively. As $2L_E$ varies, the number of the total emitter strips, N_E, varies accordingly so that $N_E L_E$ remains a constant and the total I_C remains unchanged.

Figure 5 shows the heat generation corresponding to collector currents of 50, 100, and 150 A. The heat generation rate increases with current level linearly at the BE contact and remains almost constant at the emitter center. The variation of maximum heat dissipation rate corresponding to a range of emitter width is shown in Fig. 6. For $L_E > 100$ μm, the current crowding has become well-developed and further increase of L_E does not increase heat generation significantly. However, for L_E smaller than 55 μm, the maximum heating decreases substantially with a decrease in L_E. This indicates the advantages of using narrow emitter strips to reduce heating dissipation and hot spots, as well as to increase current gain and electrical performance. The development of new technologies such as the self-aligning polysilicon technology has made it possible to fabricate emitter strips with width considerably smaller than the minimum strip width given by conventional lithography technology. Thus the quantitative correlation between heat generation and emitter strip width is quite pertinent in the design of bipolar junction transistor devices. Temperature dependency of the heat generation is also illustrated in Fig. 6, in which the collector current used is 100 A and the L_E is taken as 50 μm.

As can be seen in Fig. 6 the maximum heat dissipation rate increases linearly with an increase in device temperature. This linear dependency agrees with previous works [7, 10]. This correlation between the heat dissipation rate and the device temperature may result in a potential failure, usually termed secondary or thermal breakdown. In BJTs as well as other minority transistors, the current is carried by minority carriers and is proportional to the density of minority carriers, which in turn is proportional to $T^{1.5}$. Therefore if the temperature at one location in the transistor become higher than its surrounding, more current will flow to that location, generating more heating and thus might further increase the temperature in that area if the heat dissipation rate is greater than the heat removal rate. This results in the thermal stability problem. Temperature dependency results in Fig. 6 along with other results presented in this work can be used as an important guideline in the thermal design of BJT transistor devices.

Figure 7 displays the results of a two-dimensional thermal simulation of the BE stripe shown in Fig. 3. The half width of emitter used in the simulation is 50 μm, as measured from the device. Boundary condition used in the simulation are described below. At the symmetry lines (the base and the emitter) an adiabatic condition prevails. The heat released from the top of the device is negligible and thus the an adiabatic condition also prevails on the top. The boundary at the bottom attached to a heat sink is taken as a constant temperature condition at 80°C which represents a typical junction temperature in power transistor

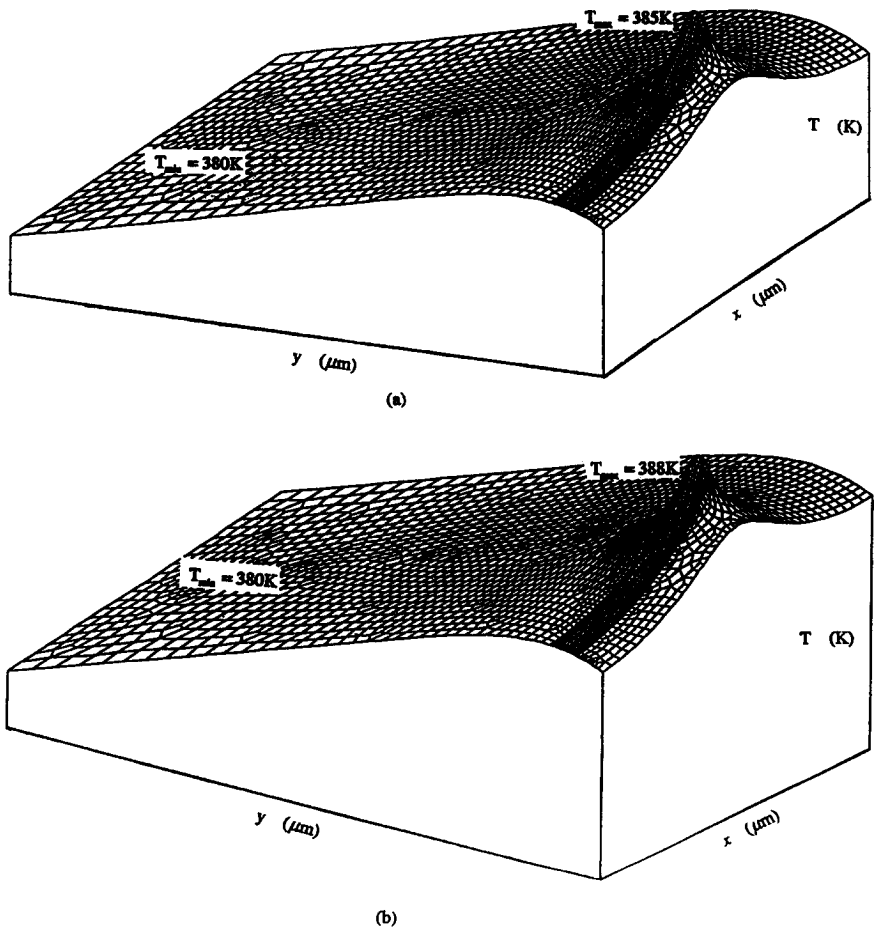

Fig. 7. Device temperature distribution (a) $I_C = 50$ A. (b) $I_C = 100$ A.

devices. Since the objectives of this study is to locate the hot spot, the relative rise of temperature from the bottom boundary temperature does not change substantially for different boundary temperatures. Figure 7 shows the temperature distribution for two different collector currents, i.e., 50 A and 100 A. The hot spot can be clearly seen in Fig. 7, localized at the BE contact region with maximum temperature rise (from boundary temperature) of 5.8 and 8.0°C for I_C values of 50 and 100 A, respectively. These local temperature rises are considerably higher than 2–3°C, previously reported by Higgins [5], where the heat generation due to emitter current crowding was not taken into consideration. It should also be noted as seen in Fig. 7 that the hot spot region is rather constrained (within 10 μm) in the x direction, implying a very large heat flux flowing in that direction.

5. CONCLUSIONS

In the study a heat generation model incorporating current crowding effects has been proposed. It is established that the heat dissipation is concentrated at the base emitter contact instead of distributing uniformly as assumed in previous models. It is found that the maximum heat generation rate drops rapidly with small emitter width whenever the half emitter width is smaller than 55 μm. As expected it is seen that the heat generation rate increases with temperature, indicating a potential thermal runaway mechanism caused by the loss of thermal stability. Hot spots associated with the localized heat generation rate are clearly observed and it is shown that the maximum temperature rise is higher than what has been reported previously. It is found that the lateral heat flux at the BE contact is very high and as such quite crucial in establishing the operating characteristics of a power device. The result of this study serves to locate potential hot spots, which must be considered to prevent thermal breakdown of power BJTs as well as other types of power devices.

Acknowledgement—The support from NASA Grant no. NCC3-324 is acknowledged and appreciated.

REFERENCES

1. Hauser, J. R., The effects of distributed base potential on emitter-current injection density and effective base

resistance for stripe transistor geometry. *IEEE Transactions of Electron Devices*, 1964, **ED-11,** 238–242.
2. Fletcher, N. H., Some aspects of the design of power transistors. *Proceedings of the Institute of Radio Engineering*, 1995, **43,** 551–559.
3. Jin, J. and Fossum, J. G., Non-quasi-static modeling/implementation of BJT current crowding for semi-numerical mixed-mode device/circuit simulation. *IEEE Transactions of CAD IC and Systems*, 1992, **11,** 759–767.
4. Mohan, N., Undeland, T. M. and Robbins, W. P., *Power Electronics, Converters, Applications and Designs*. Wiley, New York, 1995, p. 565.
5. Higgins, J. A., Thermal properties of power HBTs. *IEEE Transactions of Electron Devices*, 1993, **40,** 2171–2177.
6. Webb, P. W., Thermal modeling of power gallium Arsenide microwave integrated circuits. *IEEE Transactions of Electron Devices*, 1993, **40,** 867–877.
7. Fushinobu, K., Majumdar, A. and Hijikata, K., Heat generation and transport in submicron semiconductor devices. *Journal of Heat Transfer*, 1995, **117,** 25–31.
8. Taylor, C. and Hood, P., A numerical solution of the Navier–Stokes equations using the finite-element technique. *Computational Fluids*, 1973, **1,** 73–89.
9. *FIDAP Theoretical Manual*. Fluid Dynamics International, Evaston, IL, 1993.
10. Shaw, M. P., Mitin, V. V., Scholl, E. and Grubin, H. L., *The Physics of Instabilities in Solid State Electron Devices*. Plenum, 1992, p. 395.